



Cyclopropenone ($c\text{-C}_3\text{H}_2\text{O}$) as a Tracer of the Nonequilibrium Chemistry Mediated by Galactic Cosmic Rays in Interstellar Ices

N. Fabian Kleimeier^{1,2} , Matthew J. Abplanalp^{1,2}, Rebecca N. Johnson³, Samer Gozem³ , Joseph Wandishin⁴, Christopher N. Shingledecker^{4,5,6} , and Ralf I. Kaiser^{1,2}

¹ W. M. Keck Research Laboratory in Astrochemistry, University of Hawaii at Manoa, Honolulu, HI 96822, USA; ralfk@hawaii.edu

² Department of Chemistry, University of Hawaii at Manoa, Honolulu, HI 96822, USA

³ Department of Chemistry, Georgia State University, Atlanta, GA 30302, USA

⁴ Department of Physics and Astronomy, Benedictine College, Atchison, KS 66002, USA

⁵ Center for Astrochemical Studies, Max Planck Institute for Extraterrestrial Physics, Garching, Germany

⁶ Institute for Theoretical Chemistry, University of Stuttgart, D-85741, Stuttgart, Germany

Received 2020 July 8; revised 2021 January 12; accepted 2021 January 20; published 2021 April 12

Abstract

While gas-phase astrochemical reaction networks nicely replicate the abundance of hydrogen-deficient organics like linear cyanopolyynes, pathways to complex organic molecules (COMs)—organic molecules with six or more atoms—have not been completely understood, with gas-phase models often significantly underestimating fractional abundances of the astronomically observed organics by orders of magnitude. Here, by exploiting cyclopropenone ($c\text{-C}_3\text{H}_2\text{O}$) as a tracer, laboratory experiments on the processing of an ice mixture of acetylene (C_2H_2) and carbon monoxide (CO) by energetic electrons coupled with astrochemical model simulations expose a previously poorly explored reaction class leading to COMs via galactic cosmic-ray-mediated nonequilibrium chemistry. These processes occur within interstellar ices at ultralow temperatures, but not through traditional radical–radical pathways on grain surfaces in the warm-up phase of the ices as hypothesized for the last decades, but more likely through barrierless excited state reactions during the irradiation.

Unified Astronomy Thesaurus concepts: [Laboratory astrophysics \(2004\)](#); [Interdisciplinary astronomy \(804\)](#); [Astrochemistry \(75\)](#); [Chemical abundances \(224\)](#)

1. Introduction

Molecular clouds like the Taurus Molecular Cloud (TMC-1) have been recognized as molecular factories (Tielens 2013), aiding our understanding of the processes leading to the formation of organic molecules in the interstellar medium (ISM; Shingledecker et al. 2018; Arumainayagam et al. 2019). Because organic molecules constitute nearly 80% of the more than 200 detected interstellar and circumstellar molecules (McGuire 2018)—among them vital precursors to molecular building blocks of life such as the sugar-related glycolaldehyde (HCOCH_2OH ; Hollis et al. 2000)—the elucidation of their formation routes is important to unravel the mechanisms that drive low-temperature organic chemistry in space (Herbst 2017). Whereas gas-phase reaction networks (Herbst 2017) nicely explain the formation of highly hydrogen-deficient organics like cyanopolyynes ($\text{H}(\text{C}\equiv\text{C})_n\text{CN}$; $n = 1\text{--}5$; Jaber Al-Edhari et al. 2017) and polyynes ($\text{H}(\text{C}\equiv\text{C})_n$; $n = 1\text{--}4$; Millar et al. 2017), the pathways to complex organic molecules (COMs)—organic molecules containing six or more atoms—have remained mainly elusive, with complex gas-phase models predicting fractional abundances up to five orders of magnitudes lower than observed (Garrod et al. 2008; Abplanalp et al. 2016b; Cuppen et al. 2017).

Laboratory studies and detailed simulations (Hagen et al. 1979; Moore & Donn 1982; Bernstein et al. 1995; Herbst 2014; Boogert et al. 2015; Arumainayagam et al. 2019) indicate that the majority of COMs are likely synthesized on interstellar grains—carbonaceous and/or silicate-based nanoparticles coated with ice mantles a few hundred nanometers thick consisting of mixtures of water (H_2O), methanol (CH_3OH), carbon monoxide (CO), carbon dioxide (CO_2), methane (CH_4), formaldehyde (H_2CO), and ammonia (NH_3 ; Boogert et al. 2015). Exposure of

these ices to ionizing radiation (photons, galactic cosmic rays (GCRs)) in molecular clouds triggers the formation of COMs, some of which can be ejected from the grain nonthermally via, for instance, reactive desorption, thus enriching the gas-phase abundances of organics (Garrod et al. 2007; van Dishoeck 2014; Shingledecker et al. 2017). These processes are likely driven by reactions of atoms with excess kinetic energy (Morton & Kaiser 2003) and recombination of radicals—produced either by hydrogenation reactions (Fedoseev et al. 2015) or by interaction with ionizing radiation (Moore et al. 1996; Gerakines et al. 2001; Öberg et al. 2009; Sullivan et al. 2016; Chuang et al. 2017). Along with reactions of electronically excited atoms and molecules (Zhou et al. 2010; Paiva et al. 2018), these species can easily overcome reaction barriers (Kaiser 2002). Under interstellar conditions, the molecular synthesis advances either at 10 K within the ices and/or thermally through radical–radical recombination once the ices warm up in the hot core stage when the radicals are able to diffuse within the ices as well as on the grain surface (He et al. 2018; Arumainayagam et al. 2019; Martín-Doménech et al. 2020; Leroux & Krim 2021). The relative contribution of thermal versus nonthermal processes with regards to COM abundances is still far from being resolved; however, a growing number of observations of COMs in cold cores like TMC-1 (Öberg et al. 2010; Bacmann et al. 2012; Cernicharo et al. 2012; Jiménez-Serra et al. 2016; McGuire et al. 2018) suggest that the nonthermal formation mechanisms can be more efficient at low temperatures than has previously been assumed.

Here, we present surface-science experiments complemented by astrochemical modeling on the formation of cyclopropenone ($c\text{-C}_3\text{H}_2\text{O}$) and its isomer propynal (HCCCHO ; (Figure 1) in interstellar model ices comprised of acetylene (C_2H_2) and

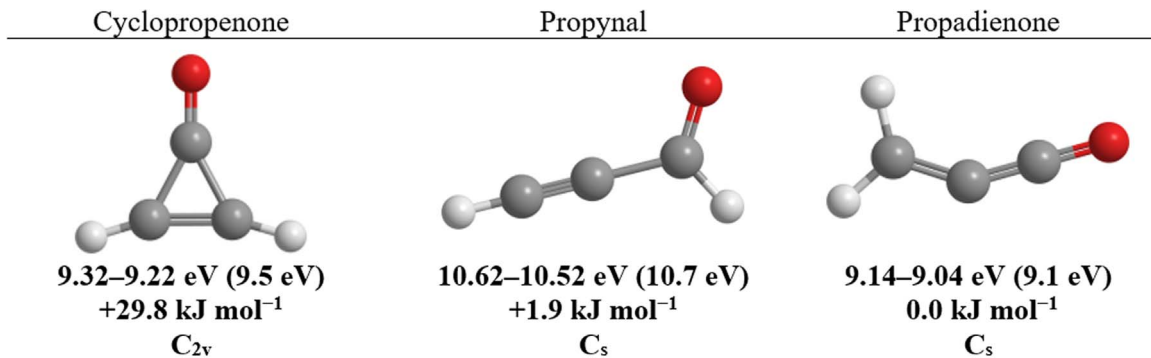
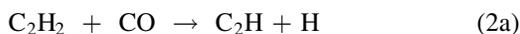


Figure 1. Structures of the C₃H₂O isomers along with their experimental ionization energies (eV), computed adiabatic ionization energies (given in parentheses), relative free energies (kJ mol⁻¹), and point groups (Harshbarger et al. 1974; von Niessen et al. 1980; Terlouw et al. 1983). The experimental ionization energies were corrected for the Stark effect.

carbon monoxide (CO) via reactions (1) and (2):



Cyclopropenone is revealed to act as a key tracer of (cyclic) COMs synthesized via GCR-triggered nonequilibrium chemistry within interstellar ices in molecular clouds at temperatures as low as 10 K. Our study may define cyclopropenone as a simple representative example of a class of COMs generated via nontraditional, low-temperature chemistry on interstellar grains by electronic excitation, which, in cold cores like TMC-1, can be accompanied by subsequent nonthermal ejection into the gas phase via, e.g., reactive desorption. These experiments were carried out in an ultrahigh vacuum (UHV) surface-science chamber at pressures of a few 10⁻¹¹ Torr by exposing C₂H₂:CO and C₂D₂:C¹⁸O ice mixtures to electrons at 5 K (Table 1).

The processing of the apolar ices with energetic electrons simulates the interaction of ices with secondary electrons generated by GCRs upon penetrating interstellar grains for a few million years (Strazzulla & Johnson 1991), thereby mimicking the exposure of apolar interstellar ices over typical lifetimes of interstellar ices in cold molecular clouds. The chemical modifications of the ices and the appearance of functional groups were traced online and in situ via Fourier transform infrared spectroscopy (FTIR; Nicolet 6700; Figure 2; Tables 2, 3). After each irradiation, the ices were warmed to 300 K to release the molecules into the gas phase (temperature-programmed desorption, TPD). During the TPD process individual subliming molecules were ionized via single-photon vacuum ultraviolet (VUV) photoionization and mass-resolved in a reflectron time-of-flight mass spectrometer (Figure 3). These apolar model ices composed of carbon monoxide with acetylene under anhydrous conditions were selected to investigate to what extent cyclopropenone and its isomer propynal are formed via interaction with ionizing radiation. Ices containing carbon monoxide at levels of up to 50% were observed toward young stellar objects (YSOs) like R Coronae Australis IRS 2 (Gibb et al. 2004). Acetylene has not yet been detected on interstellar grains, but laboratory experiments demonstrate that it can be formed easily by subjecting methane (CH₄)-bearing ices to ionizing radiation

Table 1

Data Applied to Calculate the Average Dose per Molecule from the Electron Irradiation in the Isotopically Labeled C¹⁸O:C₂D₂ Ice

Parameter	Value
Initial kinetic energy of the electrons, keV	5
Irradiation current, nA	20 ± 2
Total number of electrons	(1.1 ± 0.1) × 10 ¹⁴
Average kinetic energy of back-scattered electrons, ^a keV	3.4 ± 0.3
Fraction of backscattered electrons ^a	0.36 ± 0.03
Average kinetic energy of transmitted electrons, ^a keV	0.9 ± 0.3
Fraction of transmitted electrons ^a	0.01 ± 0.01
Average penetration depth, ^a nm	340 ± 40
Density of the mixed ice, g cm ⁻³	0.89 ± 0.27
Irradiated area, cm ²	1.0 ± 0.1
Ice constituent	C ¹⁸ O C ₂ D ₂
Total molecules processed	(6.1 ± 0.9) × 10 ¹⁷ (6.5 ± 1.2) × 10 ¹⁷
Dose per molecule, eV	0.7 ± 0.1 0.6 ± 0.1

Note.

^a CASINO values.

(Abplanalp et al. 2018b); apolar mixtures of carbon monoxide with methane at levels of up to 11% were confirmed observationally (Boogert et al. 2015).

2. Experimental

The experimental apparatus consists of a contamination-free UHV chamber operating at base pressures of a few 10⁻¹¹ Torr (Kaiser et al. 2014). Utilizing a closed-cycle helium compressor (Sumitomo Heavy Industries, RDK-415E), the substrate, a 1 cm² silver mirror interfaced to a cold finger designed from oxygen-free high-conductivity copper with a 0.2 mm sheet of indium foil to promote thermal conductivity, was cooled to 5.0 ± 0.1 K. The substrate can be rotated in its horizontal plane by using a doubly differentially pumped rotational feedthrough (Thermionics Vacuum Products, RNN-600/FA/MCO) or translated vertically via a movable UHV compatible bellow (McAllister, BLT106). The ices were prepared by depositing gas mixtures of acetylene (AirGas) and carbon monoxide (Sigma Aldrich) via a glass capillary array at a background pressure of 5 × 10⁻⁸ Torr over a few minutes (Maity et al. 2014). A dry ice-ethanol slush bath combined with a zeolite

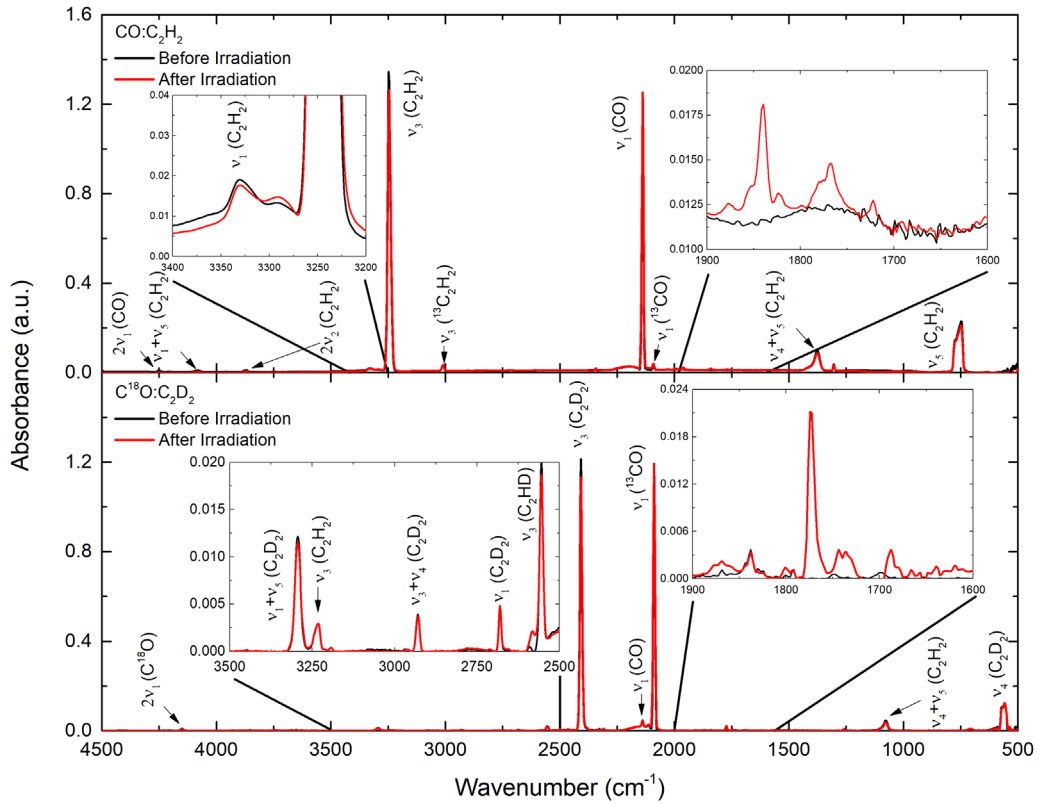


Figure 2. Infrared spectra of CO:C₂H₂ (top) and C¹⁸O:C₂D₂ (bottom) ices before (black) and after (red) the electron irradiation with assignments given in Tables 2, 3.

absorber cartridge (Chromatography Research Systems, Model 300) was utilized to remove trace amounts of the stabilizer, acetone (CH₃COCH₃), from the acetylene gas prior to mixing it with the carbon monoxide gas. Isotopically labeled ¹⁸O-carbon monoxide (C¹⁸O, 95% ¹⁸O, Sigma Aldrich) and acetylene-d₂ (C₂D₂, 99% D, CDN isotopes) ices were also investigated to confirm product assignments based on their respective isotopic shifts via FTIR and photoionization reflectron time-of-flight mass spectrometry (PI-ReTOF-MS).

The ice thickness was determined in situ to be 800 ± 50 nm by monitoring the deposition using laser interferometry with a helium–neon (HeNe) laser (CVI Melles-Griot; 25-LHP-230) operating at 632.8 nm, using an index of refraction of the mixed C₂H₂:CO ice of 1.32 ± 0.02 . An ice ratio of (1.1 ± 0.5) : (1.0 ± 0.3) for C₂H₂:CO was determined utilizing unique infrared features at 2139 cm⁻¹ (ν_1 , CO), 2090 cm⁻¹ (ν_1 , ¹³CO), 3240 cm⁻¹ (ν_3 , C₂H₂), and 4072 cm⁻¹ ($\nu_1 + \nu_5$, C₂H₂), and their corresponding absorption coefficients of 1.1×10^{-17} cm molecules⁻¹ (Gerakines et al. 1995), 1.3×10^{-17} cm molecules⁻¹ (Gerakines et al. 1995), 2.4×10^{-17} cm molecules⁻¹ (Hudson et al. 2014), and 2.3×10^{-19} cm molecules⁻¹ (Hudson et al. 2014), respectively.

After the deposition of an ice with a well-defined thickness was complete, it was irradiated with 5 keV electrons for 15 minutes at a current of 20 nA over a 1.0 ± 0.1 cm² area at an angle of incidence of 70° with respect to the surface normal of the substrate. These energetic electrons simulate secondary electrons formed in the track of GCRs. For the C₂H₂:CO ice, an average penetration depth of the 5 keV electrons was calculated utilizing Monte Carlo simulations (CASINO) to be 340 ± 40 nm, which is less than the thickness of the deposited ice mixtures (800 ± 50 nm), resulting in no interaction between the substrate and the electrons (Drouin et al. 2007). A dose of 0.7 ± 0.1 eV per carbon

monoxide molecule and 0.6 ± 0.1 eV per acetylene molecule for the ice mixture was also determined via the CASINO simulations. These doses were calculated utilizing a density of 0.89 g cm⁻³ for the mixed ice. The ice mixture was monitored both online and in situ before, during, and after the irradiation phase of the experiment via an FTIR spectrometer (Nicolet 6700) in the range of 4500–500 cm⁻¹ with a resolution of 4 cm⁻¹ in intervals of 2 minutes. This results in the collection of eight FTIR spectra during the 15 minute irradiation period at 5.0 K. After the irradiation the ice was sublimed via TPD to analyze any newly formed products in the gas phase via PI-ReTOF-MS by heating the substrate to 300 K at 0.5 K minutes⁻¹.

The PI-ReTOF-MS technique utilized in this work has previously been described in detail (Abplanalp et al. 2016a). Briefly, the subliming molecules were analyzed via single-photon ionization by using coherent VUV light pulsed at 30 Hz coupled with a reflectron time-of-flight mass spectrometer (Jordan TOF Products, Inc.). To produce 10.49 eV photons, the third harmonic of a Nd:YAG laser (354.6 nm; Spectra Physics, Quanta Ray PRO-250-30; 333 mJ pulse⁻¹) was frequency tripled using a pulsed jet of xenon as a nonlinear medium. To produce the other VUV energies (10.82 eV; 9.15 eV), resonant four-wave difference mixing was utilized ($\omega_{\text{VUV}} = 2\omega_1 - \omega_2$) by mixing ultraviolet (ω_1) and visible (ω_2) photons generated by a pair of Nd:YAG pumped dye lasers (Sirah Lasertechnik; Cobra-Stretch) using krypton or xenon as the nonlinear medium.

After generation of the ω_1 and ω_2 light, the laser beams were spatially overlapped through a system of dichroic mirrors that are sensitive to the wavelength needed as well as overlapped in time via a pulse delay-generator and then focused through a UV-grade fused silica window (Thorlabs; WG42012-B) using a fused silica plano-convex lens (Thorlabs LA4579; $f = 300$ mm) into the VUV generation chamber. The photons used to ionize

Table 2
Infrared Absorption Features Recorded Before and After the Irradiation of CO:C₂H₂ Ices at 5 K

Absorptions Before (cm ⁻¹)	Absorptions After (cm ⁻¹)	Assignment	Carrier	References
6470, 5190		$\nu_1 + \nu_3, 5\nu_4 + 3\nu_5$ (C ₂ H ₂)	Combination	1
4076, 3948, 3863		$\nu_1 + \nu_5, 2\nu_2, \nu_2 + 2\nu_4 + \nu_5$ (C ₂ H ₂)	Combination/ Overtone	1
4248		$2\nu_1$ (CO)	Overtone	2, 3, 4
3328		ν_1 (C ₂ H ₂)	CH stretch	1
	3320	ν_4 (C ₄ H ₂)	CH stretch	5
	3285	ν_1 (C ₄ H ₄); ν_1 (HC ₃ HO)	C=C–H stretch	2, 6, 7, 8
3246		ν_3 (C ₂ H ₂)	CH stretch	1
	3141	ν_{CH} (R-CHCH ₂)	CH ₂ asymmetric stretch	3, 8
3010		ν_3 (¹³ C ₂ H ₂)	CH stretch	1
	2978	ν_{10} (C ₂ H ₆);	CH ₃ degenerate stretch/CH ₂ symmetric stretch/combination	8, 9, 10
		ν_{11} (C ₂ H ₄);		
		$\nu_6 + \nu_7$ (C ₄ H ₄)		
2735, 2708		$\nu_2 + \nu_5$ (C ₂ H ₂)	Combination	4, 11
	2250	ν_1 (C ₃ O)	CO stretch	10, 12
2138		ν_1 (CO)	CO stretch	2, 3, 4
	2117	ν_3 (HC ₃ HO)	C=C stretch	6
2091		ν_1 (¹³ CO)	CO stretch	2, 3, 4
1989		ν_2 (C ₂ H ₂)	C=C stretch	4
	1877	ν_{CO} (methyl ketones)	CO stretch	10
	1853	ν_3 (HCO)	CO stretch	3, 13
	1840	ν_2 (<i>c</i> -C ₃ H ₂ O)	CO stretch	10
	1782	$2\nu_{11}$ (<i>c</i> -C ₃ H ₂ O)	Overtone	10
	1720	ν_{CO} (ketones/aldehydes)	CO stretch	3, 14, 15
1375		$\nu_4 + \nu_5$ (C ₂ H ₂)	Combination	11
	1240	$2\nu_{17}$ (C ₄ H ₄); $\nu_6 + \nu_8$ (C ₄ H ₂)	Overtone/Combination	2, 4, 8, 16
	1100-1050	ν_{CH} (Aromatic)	Out-of-plane CH deformation modes in substituted benzenes and PAHs	7, 15, 17, 18, 19, 20, 21
748		ν_5 (C ₂ H ₂)	CCH bend	1

References. (1) Hudson et al. (2014), (2) Cuyllé et al. (2014), (3) Allamandola et al. (1989), (4) Doney et al. (2018), (5) Zhou et al. (2009), (6) Hudson & Gerakines (2019), (7) Kaiser & Roessler (1998), (8) Zhou et al. (2010), (9) Abplanalp & Kaiser (2017), (10) Zhou et al. (2008), (11) Bottger & Eggers (1964), (12) Jamieson et al. (2006), (13) Duley & Anming (2009), (14) Kim & Kaiser (2009), (15) Cané et al. (1997), (16) Zhou et al. (2009), (17) Kaiser & Roessler (1997), (18) McMurtry et al. (2016), (19) Sandford et al. (2004), (20) Hudgins & Sandford (1998), (21) Kaiser et al. (1997).

subliming molecules in the main chamber were spatially separated with an off-axis lithium fluoride (LiF) biconvex lens (LiF; ISP Optics, LiF-L-38.1-3). The selected wavelength was then utilized to photoionize the subliming molecules 1 mm above the substrate surface. These ions were then analyzed within the reflectron time-of-flight mass spectrometer and detected by a multichannel plate operating in a dual chevron configuration based upon the arrival time. The multichannel plate signals were amplified (Ortec 9305) and shaped, and the time-of-flight signal was recorded via a personal computer multichannel scalar (FAST ComTec, P7888-1 E) that operated at 30 Hz (Quantum Composers, 9518) with a 4 ns bin width and 3600 sweeps for each mass spectrum, corresponding to one integrated mass spectrum recorded per Kelvin.

3. Astrochemical Model Description

In order to test the effect of the radiation-induced chemical formation routes of C₃H₂O isomers, we ran simulations of TMC-1 which include these fast, nonthermal reactions. For this, we used the three-phase—gas, grain surface, bulk ice—rate-based kinetic model NAUTILUS v 1.1 (Ruaud et al. 2016), which has previously been modified to include GCR-driven radiation chemistry (Shingledecker & Herbst 2018; Shingledecker et al. 2018). A more detailed description of how grain-surface and

ice-bulk chemistry is treated in our model can be found in Shingledecker et al. (2018).

These models employed physical conditions appropriate for TMC-1, shown in Table 4. Among the parameters used in our simulations, a reactive desorption efficiency of 1% was chosen (Garrod et al. 2007) along with initial elemental abundances taken from Hincelin et al. (2011) including a C/O value of 0.7 (Majumdar et al. 2016). The 1% input parameter is the standard value extracted by Garrod et al. (2007), while other modeling studies, such as that of Vasyunin & Herbst (2013), found overall best agreement using a higher value of 10%—though the use of this value did not universally lead to better agreement with observations for all species.

Following Shingledecker et al. (2018), our chemical network includes the GCR-driven dissociation of ice mantle species. In previous work, we examined the sensitivity of the radiation chemistry stimulated by cosmic rays on variations in the cosmic-ray ionization rate, ζ , another poorly constrained parameter in our model (Shingledecker et al. 2018). Here, we adopt the customary value of $\zeta = 1.3 \times 10^{-17} \text{ s}^{-1}$, which is almost universally used in TMC-1 simulations. To the list of radiolysis processes given in that work, we have added the dissociation of acetylene and ethylene and their product channel branching fractions. In our code, collisions between energetic particles and solid-phase species can result in the

Table 3
Infrared Absorption Features Before and After the Irradiation of C¹⁸O:C₂D₂ Ices at 5 K

Absorptions Before Irradiation (cm ⁻¹)	Absorptions After Irradiation (cm ⁻¹)	Assignment	Carrier	References
5015		$\nu_1 + \nu_3$ (C ₂ D ₂)	Combinations	1
4154		$2\nu_1$ (C ¹⁸ O)	Overtone	2, 3
3294		$\nu_1 + \nu_5$ (C ₂ D ₂)	Combinations	1
3231		ν_3 (C ₂ H ₂)	CH stretch	4
2929		$\nu_3 + \nu_4$ (C ₂ D ₂)	Combination	1
2680		ν_1 (C ₂ D ₂)	CD stretch	1
	2585	ν_4 (C ₄ D ₂)	CD stretch	5
	2573	ν_4 (C ₄ D ₄)/ ν_1 (DC ₃ D ¹⁸ O)	CD stretch	6
2555		ν_3 (C ₂ DH)	CD stretch	1
2408		ν_3 (C ₂ D ₂)	CD stretch	7, 8, 9
2341		ν_3 (¹³ C ₂ D ₂)	CD stretch	1
2325		$\nu_2 + \nu_5$ (C ₂ D ₂)	Combination	1
	2232	ν_{10} (C ₂ D ₆); ν_{11} (C ₂ D ₄)	CD ₃ degenerate stretch/ CH ₂ symmetric stretch	9, 10, 11
2139		ν_1 (CO)	CO stretch	12
2088		ν_1 (C ¹⁸ O)	CO stretch	2, 3
2037		ν_1 (¹³ C ¹⁸ O)	CO stretch	2, 3
	1969	ν_3 (DC ₃ D ¹⁸ O)	C=C stretch	13
	1800	ν_{CO} (methyl ketones)	CO stretch	
	1773	ν_3 (DC ¹⁸ O)	CO stretch	14
	1740	ν_2 (<i>c</i> -C ₃ D ₂ O ¹⁸)	CO stretch	15
	1687	ν_{CO} (ketones/aldehydes)	CO stretch	
1085		$\nu_4 + \nu_5$ (C ₂ D ₂)	Combination	1
707		ν_5 (C ₂ D ₂)	CH bend	1
565		ν_4 (C ₂ D ₂)	CD bend	1

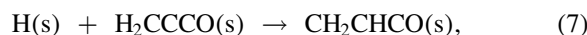
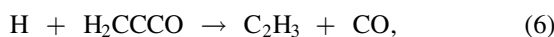
References. (1) Bottger & Eggert (1964), (2) Doney et al. (2018), (3) Duley & Anming (2009), (4) Hudson et al. (2014), (5) Wu & Cheng (2008), (6) Tjørneng et al. (1980), (7) Allamandola et al. (1989), (8) Abplanalp & Kaiser (2017), (9) Abplanalp et al. (2018b), (10) Hudgins & Sandford (1998), (11) Cané et al. (2007), (12) Cuyllé et al. (2014), (13) Hudson & Gerakines (2019), (14) Kim & Kaiser (2009), (15) Zhou et al. (2008).

formation of electronically excited and/or suprathermal reactants, which are essential for reproducing the fast, low-temperature chemistry inferred from experiments such as this (Shingledecker & Herbst 2018).

We further added the three C₃H₂O isomers to our chemical network, as well as relevant reactions taken from a recent study (Loison et al. 2016), which includes destruction in the gas phase by ions. Based on the results of their simulations, Loison et al. (2016) found that the main formation routes for propynal (HCCCHO), cyclopropenone (*c*-C₃H₂O), and propadienone (H₂CCCO) were, respectively,



However, reaction (4) has been omitted from the current model as it has not been experimentally proven to be barrierless. Although the lack of a barrier was speculated by Loison et al. (2016), the aromaticity of *c*-C₃H₂ implies a delocalization of the electron density, therefore likely resulting in a significant barrier at 10 K. We have also included the following destruction pathways for propadienone (H₂CCCO) based on recent quantum chemical calculations (Shingledecker et al. 2019):



which were found to occur barrierlessly for propadienone but not for propynal (HCCCHO). Here, reaction (6) is a gas-phase

process, while reaction (7) occurs on grains. Finally, based on the experimental results described below, we added non-thermal formation routes for propynal and cyclopropenone (*c*-C₃H₂O).

4. Quantum Mechanical Calculations

4.1. Ionization Energies and Relative Energies

The coupled-cluster with single, double, and perturbative triple excitations (CCSD(T)) and the aug-cc-pVTZ basis set were used to optimize the following using the finite-difference approach for the gradient: (1) the ground singlet states of cyclopropenone (*c*-C₃H₂O), propynal (HCCCHO), and propadienone (H₂CCCO); (2) the ionized states, which are doublet cations; and (3) triplet states starting from the singlet optimized geometry to rule out low-lying triplet states in those molecules. Singlet, doublet cation, and triplet-state geometries for all three systems were used as a starting point for the W1 protocol (Martin & de Oliveira 1999) as implemented in Gaussian (Frisch et al. 2016), keeping the geometries at the CCSD(T) optimized geometries. The relative free energies and adiabatic ionization energies computed using this protocol are reported in Figure 1.

The singlet–triplet adiabatic energy difference for HCCCHO and H₂CCCO are 3.0 eV and 1.7 eV, respectively, meaning that their triplet state is considerably higher in energy than the ground-state singlet for both systems. In the case of *c*-C₃H₂O, the triplet state is dissociative, and optimization on the triplet potential energy surface leads to

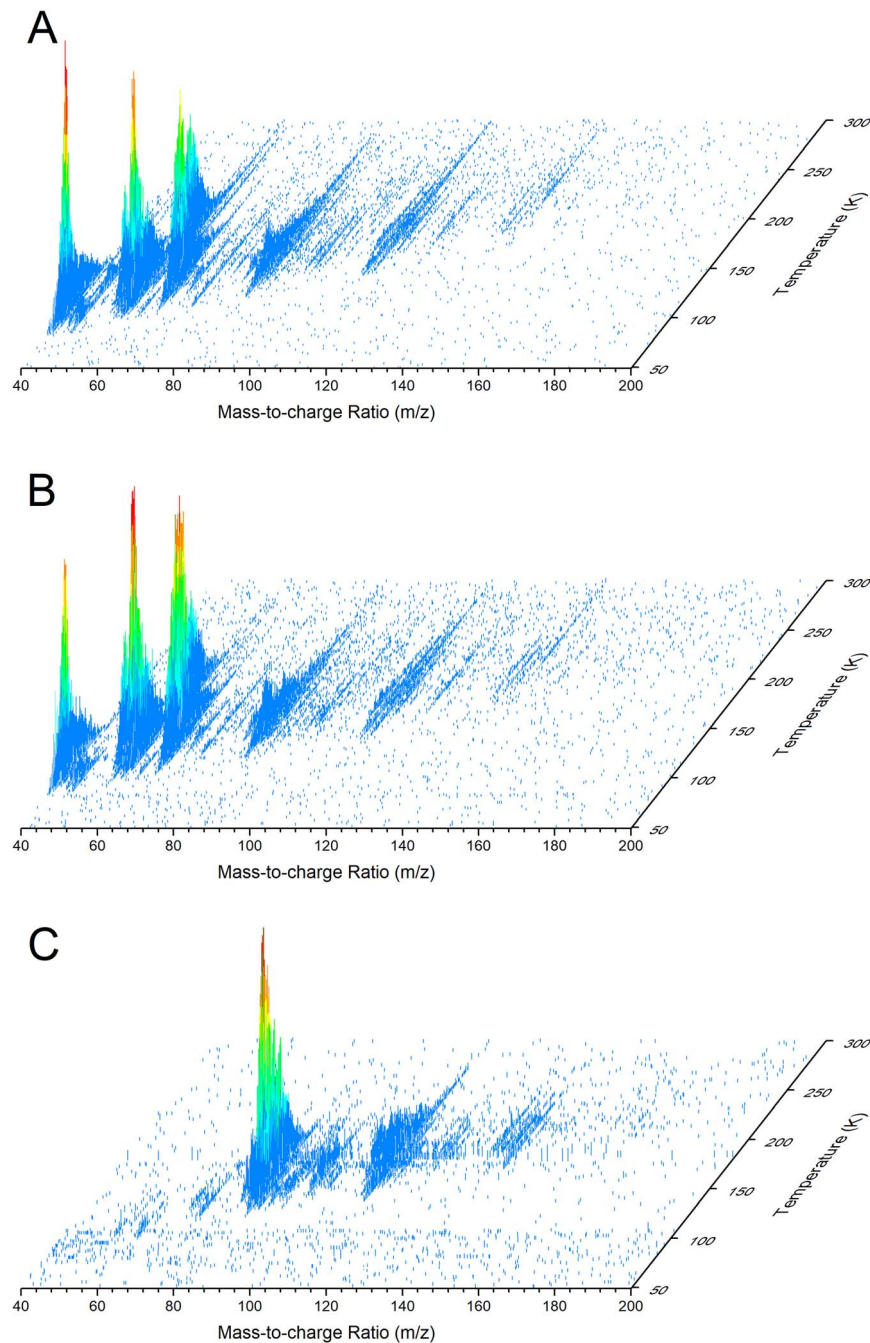


Figure 3. PI-ReTOF-MS data displaying ion counts as a function of temperature of the newly formed products of processed $C^{18}O:C_2D_2$ ices subliming into the gas phase utilizing photoionization energies of 10.82 eV (A), 10.49 eV (B), and 9.20 eV (C).

Table 4

Model Parameters and Physical Conditions Utilized in the Astrochemical Network

Parameter	Value
Gas density (n_H ; cm^{-3})	10^4
Gas temperature (T_{gas} ; K)	10
Grain temperature (T_{grain} ; K)	10
Extinction (A_V ; mag)	10
Cosmic-ray ionization rate (ζ ; s^{-1})	1.3×10^{-17}

the breaking of one of the carbonyl- CH_2 bonds. All CCSD(T) optimizations carried out in this work were performed in Q-Chem. (Shao et al. 2015).

4.2. Photoionization Cross Sections

To get an order-of-magnitude estimate of branching ratios from experimental photoionization yields, we computed approximate photoionization cross sections for $c\text{-}C_3H_2O$, $HCCCHO$, and H_2CCCO using a protocol previously reported (Abplanalp et al. 2016b; Table 5). Briefly, the molecules were optimized using coupled-cluster with single and double excitations (CCSD) and the cc-pVTZ basis set (Purvis & Bartlett 1982; Dunning 1989). Dyson orbitals were then computed with the equation-of-motion ionization potential at the EOM-IP-CCSD/aug-cc-pVTZ level of theory (Stanton & Gauss 1994). In addition to the Dyson orbitals, which contain all the necessary information about the molecular system (Ortiz 1999; Oana & Krylov 2007;

Table 5
Calculated Photoionization Cross Sections at 10.82 eV Ionizing Radiation

Effective Charge (Z_{eff})	Cyclopropenone (Mb)	Propynal (Mb)	Propadienone (Mb)
0.0	3.15	0.98	5.85
0.2	4.76	4.42	9.07
0.4	9.92	8.43	9.00
0.6	15.16	8.64	8.81
0.8	17.17	6.72	9.46
1.0	15.18	5.10	10.28

Note. 1 Mb = 10^{-18} cm².

Gozem et al. 2015), cross-section calculations also require the photoelectron wave function. Solving for the photoelectron wave function while accounting for the effect of the ionized core is not trivial, so a plane wave or Coulomb wave is often employed. Previous studies have indicated that, for molecules, a Coulomb wave with a partial (effective) charge Z_{eff} between 0 and 1 gives cross sections that are in good agreement with the experimental values (Gozem et al. 2015, 2020; Abplanalp et al. 2016b). However, an approach for predicting Z_{eff} from first principles is not yet available. Instead, to get an approximation of photoionization cross sections in this work, we compute the cross sections of each isomer at six values of Z_{eff} (0, 0.2, 0.4, 0.6, 0.8, 1.0) and take their average, as done in Abplanalp et al. (2016b).

These calculations allow us to estimate the uncertainty based on the maximum and minimum values of the cross sections obtained at different Z_{eff} values. The effect of Franck–Condon factors (FCFs) on the photoionization cross sections is also included in the calculation of the photoionization cross sections following the protocol outlined by Oana & Krylov (2009) and Gozem et al. (2015) (Table 5). FCFs were computed within the double-harmonic and parallel-mode approximations based on ground-state CCSD and ionized-state EOM-IP-CCSD geometries and unscaled frequencies (Mozhayskiy & Krylov 2008). The final cross sections and uncertainties were used to compute branching ratios, as discussed in Section 5. All electronic structure calculations in this section were performed with Q-Chem (Shao et al. 2015). Photoionization cross sections were computed with ezDyson v4.3 (Gozem & Krylov 2018). FCFs were computed with ezSpectrum v 3.0 (Mozhayskiy & Krylov 2008).

5. Results and Discussion

5.1. Infrared Spectroscopy

The infrared spectra of the electron-irradiated $\text{C}_2\text{H}_2:\text{CO}$ and $\text{C}_2\text{D}_2:\text{C}^{18}\text{O}$ ices revealed notable functional groups at 5 K related to the $\text{C}_3\text{H}_2\text{O}$ isomers (Figure 2; Tables 2, 3). These absorptions might be linked to the carbonyl group ($\text{C}=\text{O}$) of cyclopropenone (ν_2 , 1840 cm⁻¹; Yang et al. 2004) and an acetylenic C–H stretch ($\text{C}=\text{C}-\text{H}$) as well as a C=C stretch with respect to propynal (ν_1 , 3285 cm⁻¹; ν_3 , 2117 cm⁻¹; Hudson & Gerakines 2019). The isotopic experiments ($\text{C}^{18}\text{O}:\text{C}_2\text{D}_2$) verified these assignments with absorptions shifted to 1740 cm⁻¹ (ν_2 , *c*- $\text{C}_3\text{D}_2^{18}\text{O}$) (Yang et al. 2004), 2573 cm⁻¹ (ν_1 , $\text{DC}_3\text{D}^{18}\text{O}$), and 1969 cm⁻¹ (ν_3 , $\text{DC}_3\text{D}^{18}\text{O}$; Zhou et al. 2008). Functional groups corresponding to the propadienone isomer could not be assigned.

These detections indicate that functional groups associated with cyclopropenone and propynal are produced via the exposure of the ices to ionizing radiation at 5 K. However,

considering that infrared spectroscopy is only able to verify functional groups and that these functional groups often overlap if multiple complex organics are produced, FTIR does not always allow an unambiguous identification of the individual isomers of COMs in complex mixtures of organics (Abplanalp et al. 2016a). Nevertheless, it is important to note that FTIR can identify small molecules; the formyl radical (HCO , ν_3 , 1853 cm⁻¹)—an important species for the synthesis of carbonyl-containing COMs (Abplanalp et al. 2018a)—was confirmed via its isotopic shift (DC^{18}O , ν_3 , 1773 cm⁻¹).

5.2. PI-ReTOF-MS

In order to identify the individual reaction products, photoionization reflectron time-of-flight mass spectrometry (PI-ReTOF-MS) was utilized to monitor the subliming molecules during heating of the irradiated ices. The PI-ReTOF-MS technique allows for the identification of specific molecular isomers based on their distinct ionization energies (IEs) and desorption temperatures (Abplanalp et al. 2015, 2019; Kostko et al. 2016; Eckhardt et al. 2019; Figure 3). The experimental adiabatic ionization energies for propynal, cyclopropenone, and propadienone isomers (Figure 1) of 10.60 ± 0.05 eV (von Niessen et al. 1980), 9.30 ± 0.05 eV (Harshbarger et al. 1974), and 9.12 ± 0.05 eV (Terlouw et al. 1983) have to be corrected for the Stark effect induced by the electric field of the ReTOF-MS, which lowers the ionization energies by up to 0.03 eV (Zhu et al. 2019). This yields effective ionization energies for propynal, cyclopropenone, and propadienone of 10.62–10.52 eV, 9.32–9.22 eV, and 9.14–9.04 eV, respectively. Therefore, the subliming products were photoionized in separate experiments with photon energies of 10.82, 10.49, and 9.20 eV to determine which $\text{C}_3\text{H}_2\text{O}$ isomer(s) were formed.

Here, the 10.82 eV photons are capable of photoionizing all three isomers if they are formed. By tuning the photoionization energy to 10.49 eV, only the cyclopropenone and propadienone isomers can be ionized, but not the propynal isomer. Finally, the 9.20 eV photons can only photoionize propadienone, but no other $\text{C}_3\text{H}_2\text{O}$ isomer. This systematic approach allows for the determination of which isomers are formed if multiple $\text{C}_3\text{H}_2\text{O}$ isomers were synthesized in the ices. Furthermore, to assure that these subliming products can be clearly assigned to the $\text{C}_3\text{H}_2\text{O}$ isomers, isotopically labeled $\text{C}_2\text{D}_2:\text{C}^{18}\text{O}$ ices were chosen to prevent overlap with other possible products at the same mass-to-charge ratio as $m/z = 54$ is already detected in pure acetylene ices subjected to electron irradiation (Abplanalp & Kaiser 2020), whereas in ices containing only C^{18}O and deuterated hydrocarbons, $m/z = 58$ can only be due to the molecular formula $\text{C}_3\text{D}_2^{18}\text{O}$ (Figure 4) (Abplanalp & Kaiser 2019).

At a photon energy of 10.82 eV, the TPD profile of $m/z = 58$ of the irradiated ice reveals two sublimation events from 128 to 155 K and 150 to 230 K (Figure 4). Utilizing a photon energy of 10.49 eV, at which propynal cannot be ionized, the TPD profile of $m/z = 58$ exhibits only a single sublimation event from 150 to 230 K; the early sublimation event vanishes at 10.49 eV. Consequently, the 128 to 155 K sublimation event at 10.82 eV confirms the formation of propynal; the second sublimation event from 150 K to 230 K is connected to the formation of a second isomer. Lowering the photon energy to 9.20 eV, no ion counts above the background level at $m/z = 58$ are visible. Consequently, propadienone was not formed, and the 150–230 K sublimation event is linked to the formation of cyclopropenone. Therefore, both propynal and cyclopropenone are formed from the exposure of $\text{C}_2\text{H}_2:\text{CO}$ ices with energetic

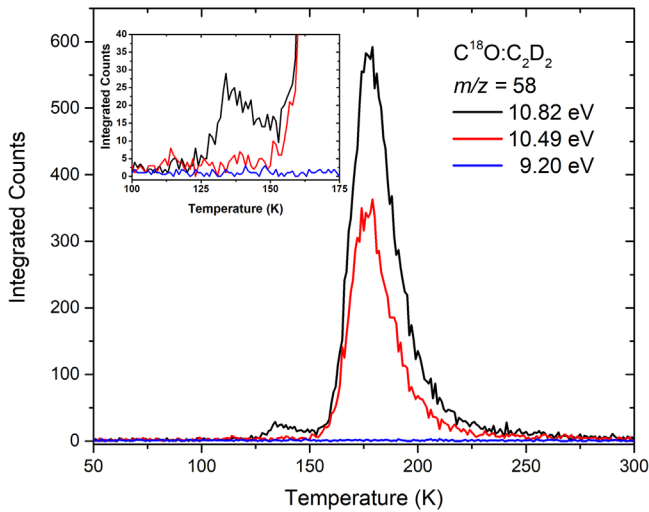


Figure 4. PI-ReTOF-MS ion signal for $m/z = 58$ ($C_3D_2^{18}O$) from electron irradiation recorded at photoionization energies of 10.82 eV (black), 10.49 eV (red), and 9.20 eV (blue).

electrons. Interestingly, only the propynal and cyclopropenone isomers have been detected in interstellar environments, while the thermodynamically most stable propadienone isomer has remained elusive (Loison et al. 2016) as mirrored in the present experiments (Shingledecker et al. 2019).

5.3. Isomer Branching Ratios

The detection of multiple isomers from the PI-ReTOF-MS studies allows for the calculation of the branching ratios of these isomers utilizing their detected signal and respective photoionization cross sections. Here, branching ratios provide valuable information on the conditions during their synthesis. If the isomers are synthesized within a thermodynamic equilibrium process during the warm up in the gas phase, i.e., a hypothetical tautomerization of the subliming propynal to cyclopropenone, this route is connected with an equilibrium constant K defined as the quotient of the concentration of the isomers with $K = [\text{propynal}]/[\text{cyclopropenone}] = \exp(-\Delta G/RT)$ at the temperature T with R being the ideal gas constant and ΔG the difference in standard Gibbs free energies of the isomers: ΔG (propynal—cyclopropenone) = $-27.9 \text{ kJ mol}^{-1}$ (Figure 1). Hence, within the temperature range from 5 K to 250 K, the former being the temperature at which the experiments were conducted and the latter defining the maximum temperature at which the isomers have sublimed, abundance ratios of 3×10^{291} (5 K) and of 7×10^5 (250 K) for propynal versus cyclopropenone would be expected.

However, a comparison of these data with the experimentally derived branching ratios of $(1.0 \pm 0.5):(15.0 \pm 8.3)$ (propynal:cyclopropenone) exposes a significant overproduction of the cyclopropenone isomer between 6 (250 K) and 292 (5 K) orders of magnitude. Therefore, our data reveal that in our experiments, these isomers are not formed under thermal equilibrium conditions within the warm-up phase of the ices but through nonequilibrium processes at ultralow temperatures. Based on the integrated ion counts and the photoionization cross sections, formation rates of propynal and cyclopropenone are determined to be $(6.1 \pm 3.1) \times 10^{-4}$ and $(9.1 \pm 4.9) \times 10^{-3}$ molecules eV^{-1} , respectively, corresponding to a ratio of $(1.0 \pm 0.5):(15.0 \pm 8.3)$ (Table 6). The units of molecules produced per eV absorbed by the ices were chosen so that these data can directly be incorporated into the astrochemical models.

Table 6
Yields of C_3H_2O Isomers Detected via PI-ReTOF-MS

Molecules	Photoionization Cross Section at 10.82 eV (Mb)	PI-ReTOF-MS Calculated Yield (molecules eV^{-1})
Propynal	5.7 ± 2.9	$6.1 \pm 3.1 \times 10^{-4}$
Cyclopropenone	10.9 ± 5.9	$9.1 \pm 4.9 \times 10^{-3}$
Relative Ratio		
Propynal : Cyclopropenone		$1.0 \pm 0.5 : 15.0 \pm 8.3$

5.4. Astrochemical Modeling

Having revealed that cyclopropenone ($c\text{-}C_3H_2O$) and propynal (HCCCCHO) are synthesized in interstellar analog ices via a GCR-mediated chemistry and nonequilibrium radical–radical recombination, respectively, these findings are now transported from the laboratory and quantum chemical calculations to a simulated interstellar environment through astrochemical models. This approach is essential because even complex laboratory experiments and computations cannot mimic the chemical and physical complexity of the ISM, generally, and of ices in particular. For example, unlike the two-component ices in this proof-of-concept study, real dust-grain ice mantles consist of a complex mixture of diverse molecules—including complex organics—dominated by water (Boogert et al. 2015), and this chemical diversity must be accounted for in the astrochemical models.

A second major difference between our well-constrained experiments and actual interstellar environments is that, in the latter, ices are processed by GCRs with a wide range of kinetic energies (Arumainayagam et al. 2019). Finally, the fluxes employed in our laboratory simulation experiments—as is the case in all similar laboratory-astrophysical simulations of interstellar ice analogs—are far greater than those of GCRs typically thought to exist in interstellar environments (Indriolo & McCall 2013). Therefore, given these differences between the experimental conditions we employ and those in the ISM, the true efficiency of the processes considered here must be explored through astrochemical modeling. Here, we utilize a complex network of gas-phase reactions and include a number of new solid-phase reactions, most importantly, the GCR-triggered synthesis of cyclopropenone ($c\text{-}C_3H_2O$) and propynal (HCCCCHO) (reactions (1)–(2); Wakelam et al. 2015).

As noted previously, in order to examine the potential importance of the chemistry described here on the synthesis of cyclopropenone and propynal, we exploited the three-phase rate equations based on the Nautilus v 1.1 code (Ruaud et al. 2016), which has been previously modified to account for GCR-driven radiation–chemical processes (Shingledecker & Herbst 2018; Shingledecker et al. 2017). Because both cyclopropenone and propynal have been observed toward the molecular cloud TMC-1, physical conditions were chosen to mimic this region of space and to explore the contributions of nonequilibrium chemistry in these environments.

First, we ran a “control” model in which we simulated quiescent isothermal average conditions with a gas density of 10^4 cm^{-3} and 10 K without the inclusion of nonequilibrium ice chemistry. This model significantly underproduced cyclopropenone by up to 12 orders of magnitude (Figure 5), with fractional abundances of 3.4×10^{-19} – 3.8×10^{-24} with respect to molecular hydrogen (H_2) being predicted in the control model, compared with observed fractional abundances toward TMC-1 of 5.4×10^{-12} (Loison et al. 2016) for cyclopropenone

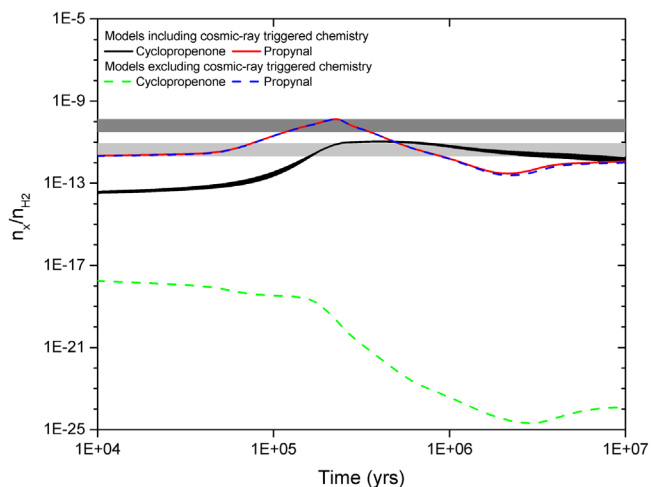


Figure 5. Astrochemical models predicting the fractional abundances of cyclopropenone and propynal in TMC-1. The models were operated with (solid lines) and without (dashed lines) a GCR-triggered chemistry and provide compelling evidence of the essential role of a GCR-driven formation of cyclopropenone within ices at 10 K. The light-gray bar defines the observed astronomical abundance of cyclopropenone in TMC-1 with 60% error limits; the dark-gray bar defines the observed astronomical abundance of propynal in TMC-1 along with 60% error limits.

at typical dense cloud ages of 10^5 – 10^6 yr (Strazzulla & Johnson 1991). In these “gas-phase and surface chemistry only” networks, cyclopropenone is mainly produced via the speculative, unstudied surface reaction of ground-state oxygen atoms with cyclopropenylydene ($c\text{-C}_3\text{H}_2$; Hollis et al. 2006), which occurs via the thermal diffusion of the reactants. Second, we conducted simulations in which the nonequilibrium chemistry described here was enabled. These models revealed that reactions (1)–(2)—followed by release into the gas phase through GCR-induced grain heating, photodesorption, and reactive desorption—provided an excellent agreement with the observed fractional abundance of cyclopropenone toward TMC-1 of 5.4×10^{-12} (Loison et al. 2016), where our models predict a peak fractional abundance of $c\text{-H}_2\text{C}_3\text{O}$ that is within observational uncertainties after a few 10^5 yr (Figure 5). We note that the range of calculated cyclopropenone abundances reflects the experimental error in the measured rate of reactions (1)–(2).

In both models, results for propynal with and without the nonequilibrium chemistry revealed only minor changes in fractional abundances and similarly show peak abundances of $\sim 10^{-10}$, which are in excellent agreement with the observed fractional abundance of propynal (8.0×10^{-11}) after 1.7×10^5 yr (Figure 5). Here, as in the work by Loison et al. (2016), propynal is produced mainly via the barrierless biomolecular gas-phase reaction of atomic oxygen with propargyl radicals (C_3H_3 ; reaction (3)). Our model results represent the best reproduction of interstellar $\text{C}_3\text{H}_2\text{O}$ abundances to date and suggest that the cyclopropenone molecule can be classified as a tracer of a vigorous GCR-induced nonequilibrium chemistry within interstellar ices. Critically, these processes occur efficiently within the ices even at 10 K deep inside molecular clouds and do not require thermal activation.

6. Astrophysical Implications

Our combined experimental, computational, and astrochemical modeling studies provide compelling evidence on facile,

GCR-triggered chemistry leading to the formation of complex organic molecules within interstellar ices in cold cores such as TMC-1, where temperatures are as low as 10 K. These processes occur at 10 K within interstellar ices and not through classical radical–radical recombination on the grain surfaces in the warm-up phase of the irradiated ices as postulated over the last decades. Instead, based on the potential energy surface and molecular structure, $c\text{-C}_3\text{H}_2\text{O}$ most likely forms by the reaction of an electronically excited molecule with a ground-state molecule as this reaction can proceed barrierlessly (Zhou et al. 2008). Due to the short lifetime of such excited states, these reactions can only happen during the irradiation phase at low temperatures and not during the warm-up phase. The implementation of the CR-driven formation rates of $c\text{-C}_3\text{H}_2\text{O}$ into novel astrochemical models reveals excellent agreement of the modeled and astronomically observed fractional abundances of $c\text{-C}_3\text{H}_2\text{O}$ toward TMC-1 by boosting the fractional abundance of cyclopropenone by up to 12 orders of magnitude, thus suggesting cyclopropenone as a potential tracer of a nonequilibrium-triggered ice chemistry.

Because the reaction of ground-state carbon monoxide with acetylene is suppressed due to a high potential barrier, electronic excitations of acetylene and/or carbon monoxide to excited singlet and triplet states are expected to play a critical role. These processes can be induced by secondary electrons generated from GCRs penetrating interstellar ices. These (short-lived) states are likely involved in the formation of cyclopropenone. Real interstellar conditions are more complex than laboratory simulation experiments, although laboratory studies are crucial to isolate and derive fundamental mechanisms by conducting proof-of-concept studies on the formation of COMs under well-defined conditions in interstellar ices. In particular, the combination of actual, verified data from laboratory experiments with astrochemical modeling exposes isomer specific routes in the condensed phase (cyclopropenone, propynal) along with their branching ratios and the complementary role of the dominating synthetic routes to cyclopropenone in the condensed phase (ices) versus propynal in the gas phase of molecular clouds and hot cores.

We acknowledge the W. M. Keck Foundation for financing the experimental setup. The experiments were supported by the US National Science Foundation (NSF) Division of Astronomical Sciences (AST) under Award 1800975 (“An Experimental Investigation of the Synthesis of Complex Organic Molecules in Interstellar Analog Ices”) to the University of Hawaii (R.I.K). Parts of the experiments and data analysis were supported by the Deutsche Forschungsgemeinschaft (DFG) through a Research Fellowship (KL 3342/1-1, N.F.K). C.N.S. thanks the Alexander von Humboldt Foundation for their generous support and V. Wakelam for use of the Nautilus-v1.1 code. S.G. acknowledges the donors of the American Chemical Society Petroleum Research Fund for support through PRF# 60837-DNI6, as well as the NSF XSEDE for computation resources through Research Allocation CHE180027.

Appendix A

Further Astrochemical Modeling Details

In this work, the third $\text{H}_2\text{C}_3\text{O}$ isomer, propadienone, was not detected in the processed ices, just as it has thus far not been detected in the ISM (Loomis et al. 2015; Loison et al. 2016). One possible explanation is that, as reported by

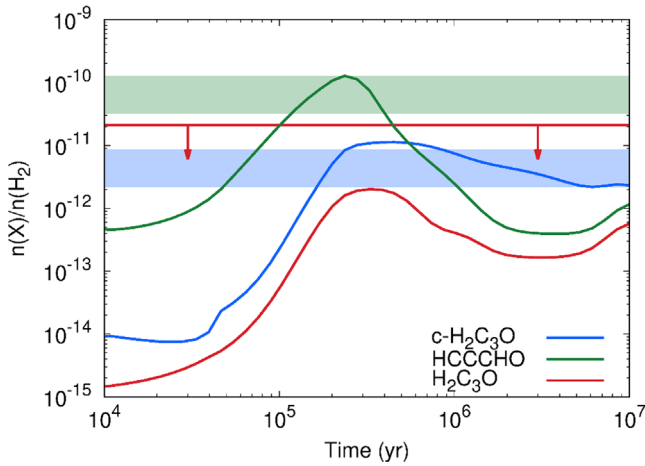


Figure A1. Astrochemical models predicting the fractional abundances of cyclopropenone, propynal, and propadienone in TMC-1. The models were operated with GCR-triggered chemistry. Horizontal bars define the observed astronomical abundances of $c\text{-H}_2\text{C}_3\text{O}$ and HCCCHO in TMC-1 with 60% error limits, while the upper limit for propadienone is given by the red line and arrows.

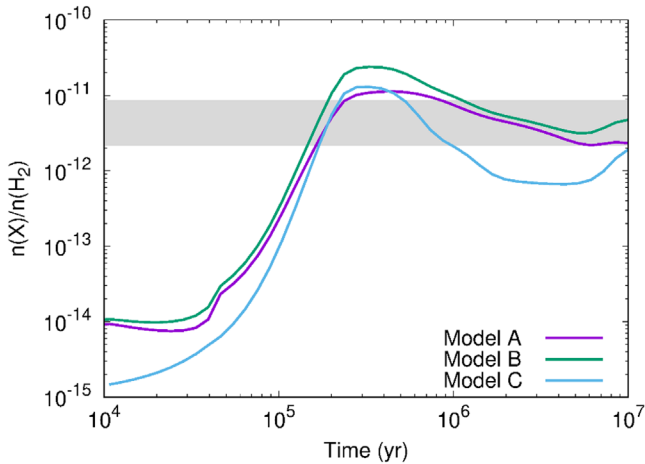


Figure A2. Calculated abundances of cyclopropenone, without reaction (4) and with GCR-driven chemistry enabled (Model A), with reaction (4) and GCR-driven chemistry enabled (Model B), and, finally, with reaction (4) and GCR-driven chemistry disabled (Model C). The observed abundances of Loison et al. (2016) are given by the horizontal bar.

Shingledecker et al. (2019), propadienone is uniquely reactive with atomic hydrogen. We incorporated some of the reactions studied in Shingledecker et al. (2019) into our network, namely, the reaction of $\text{H} + \text{HC}_3\text{O}$, which was found to yield equal amounts of propynal and propadienone, as well as $\text{H} + \text{H}_2\text{C}_3\text{O}$ in both the gas and on grains. Calculated abundances for all three $\text{H}_2\text{C}_3\text{O}$ isomers, as well as the

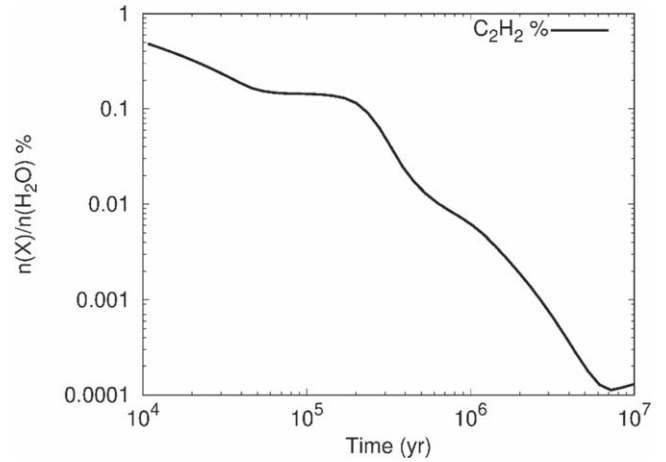


Figure A3. Calculated abundances of solid-phase acetylene (C_2H_2) relative to water in our simulations.

observational values and upper limits, are given in Figure A1. There, one can see that the fractional abundance of propadienone remains at least one order of magnitude below the observational upper limit of 2.1×10^{-11} (Loison et al. 2016) at all model times.

As noted in the main text, we have not included the proposed cyclopropenone formation route between OH and $c\text{-C}_3\text{H}_2$, given in reaction (4), which has not been experimentally studied. However, to illustrate its effects in our simulations, we show in Figure A2 the results of three model runs labeled A, B, and C. In Model A, we include GCR-driven chemistry but not reaction (4). In Model B we include both reaction (4) and GCR-driven radiation chemistry. Finally, in Model C, we include reaction (4) but have disabled GCR-driven radiation chemistry. From Figure A2 one can see that overall best agreement with observations over the longest time is obtained in Model A.

Finally, in Figure A3, we show the abundance of acetylene in the ice relative to water. One can see there that at relevant model times greater than 10^5 yr, the fraction of C_2H_2 in the ice relative to water never exceeds 0.1%. Because the observational limit of species thus far detected in cosmic ices is on the order of 0.5%–1% (Boogert et al. 2015) and because acetylene, to the best of our knowledge, has not been detected, its abundance should be lower than this approximate detection limit—which is encouragingly what we find from Figure A3.

Appendix B Quantum Mechanical Calculations Data

The computed absolute free energies and vibrational frequencies of $\text{C}_3\text{H}_2\text{O}$ molecules are presented in Tables B1 and B2, respectively.

Table B1Absolute Free Energies of Cyclopropanone ($c\text{-C}_3\text{H}_2\text{O}$), Propynal (HCCCHO), and Propadienone (H_2CCCO) Computed Using the W1 Protocol on top of CCSD(T) Optimized Geometries

	$c\text{-C}_3\text{H}_2\text{O}$	HCCCHO	H_2CCCO
Free energy, S_0 state, Hartree	-190.705910	-190.716563	-190.717269
Free energy, D_1 state, Hartree	-190.356713	-190.323511	-190.382610
Free energy, T_1 state, Hartree	N/A	-190.605629	-190.655178

Note. Shown are energies for the singlet ground state (S_0), ionized state (D_1), and first triplet excited state (T_1). The triplet state for $c\text{-C}_3\text{H}_2\text{O}$ could not be optimized due to bond dissociation on the triplet surface.

Table B2Computed Vibrational Frequencies for $c\text{-C}_3\text{H}_2\text{O}$, HCCCHO, and H_2CCCO in the S_0 and D_1 States

$c\text{-C}_3\text{H}_2\text{O}$, S_0 (cm^{-1})	$c\text{-C}_3\text{H}_2\text{O}$, D_1 (cm^{-1})	HCCCHO, S_0 (cm^{-1})	HCCCHO, D_1 (cm^{-1})	H_2CCCO , S_0 (cm^{-1})	H_2CCCO , D_1 (cm^{-1})
485	378	273	130	254	178
532	506	332	287	314	227
770	717	652	414	578	449
814	793	688	746	738	604
851	832	749	844	1028	906
985	865	1008	912	1068	1022
1133	981	1135	1175	1410	1207
1142	1059	1410	1493	1660	1760
1878	1623	1826	1900	2027	2088
3174	3138	2940	2840	3080	3041
3176	3173	3419	3353	3161	3131

Optimized Coordinates

$c\text{-C}_3\text{H}_2\text{O}$, S_0 , CCSD(T)/aug-cc-pVTZ			
C	0.3281182423	0.0000052525	0.0000009792
C	-0.9401034399	0.6765179240	-0.0000009106
C	-0.9400871847	-0.6765243077	-0.0000002424
O	1.5348556763	0.0000041491	0.0000019929
H	-1.5709239991	1.5550331075	-0.0000253056
H	-1.5708520262	-1.5550816894	-0.0000228016
$c\text{-C}_3\text{H}_2\text{O}$, D_1 , CCSD(T)/aug-cc-pVTZ			
C	0.3445264139	-0.0000381051	-0.0000047305
C	-0.9554721537	0.6580208898	-0.0000891813
C	-0.9554554418	-0.6579942367	0.0000852051
O	1.5320291105	-0.0000108407	0.0000034143
H	-1.3982061197	1.6482161419	0.0000375395
H	-1.3982044065	-1.6481777668	-0.0000322472
HCCCHO, S_0 , CCSD(T)/aug-cc-pVTZ			
C	0.7342702956	0.4154922674	-0.0000444114
C	-0.6838528757	0.0845164136	0.0000123047
C	-1.8778861684	-0.1324328766	-0.0000767731
O	1.6168548677	-0.4193235405	0.0000385663
H	-2.9206181045	-0.3485580992	-0.0000909696
H	0.9603382493	1.4928493572	-0.0001684600
HCCCHO, D_1 , CCSD(T)/aug-cc-pVTZ			
C	0.6957670395	0.4243945598	-0.0006254640
C	-0.6615836998	0.1046960741	-0.0018621458
C	-1.8481029498	-0.1448887637	0.0040527515
O	1.5918781452	-0.4340531938	0.0002520540
H	-2.8976727383	-0.3661245814	0.0058285678
H	1.0719584667	1.4668128005	-0.0003735708
HCCCHO, T_1 , CCSD(T)/aug-cc-pVTZ			
C	0.6391917077	0.5108164121	0.0024725604
C	-0.7150770343	0.1522458110	-0.0133519605
C	-1.9128905204	-0.1738608163	0.0290516743

(Continued)

O	1.5974923554	-0.4387668164	-0.0048308035
H	-2.9540471044	-0.4430628921	-0.0344135959
H	1.0233001658	1.5381355299	-0.0179251994
H_2CCCO , S_0 , CCSD(T)/aug-cc-pVTZ			
C	1.8079519243	-0.1670191096	-0.0003219553
C	0.5789287610	0.3603523981	-0.0002000049
C	-0.6870373288	0.0021544518	-0.0000034134
O	-1.8573539450	-0.0589055024	0.0001682685
H	2.6848598416	0.4730133330	-0.0003041645
H	1.9872572618	-1.2394743187	-0.0001100650
H_2CCCO , D_1 , CCSD(T)/aug-cc-pVTZ			
C	-1.8811567479	-0.0001260987	0.0001200983
C	-0.5745260309	0.0004310267	-0.0002966591
C	0.7533279480	-0.0002011563	-0.0001274127
O	1.8936963199	0.0000389656	0.0001574582
H	-2.4386151817	0.9393167455	0.0001822959
H	-2.4378425144	-0.9400335086	0.0001810639
H_2CCCO , T_1 , CCSD(T)/aug-cc-pVTZ			
C	1.8939389451	-0.1837342060	-0.0000369608
C	0.5181400935	-0.0585334559	-0.0000383538
C	-0.7786927952	0.0578342579	-0.0000834109
O	-1.9751284730	0.1663643971	0.0001184056
H	2.5288978695	0.7080948453	-0.0009312965
H	2.3577292709	-1.1754332991	0.0004266180

ORCID iDs

N. Fabian Kleimeier  <https://orcid.org/0000-0003-1767-897X>Samer Gozem  <https://orcid.org/0000-0002-6429-2853>Christopher N. Shingledecker  <https://orcid.org/0000-0002-5171-7568>Ralf I. Kaiser  <https://orcid.org/0000-0002-7233-7206>

References

- Abplanalp, M. J., Borsuk, A., Jones, B. M., & Kaiser, R. I. 2015, *ApJ*, **814**, 45
- Abplanalp, M. J., Förstel, M., & Kaiser, R. I. 2016a, *ChPhL*, **644**, 79
- Abplanalp, M. J., Góbi, S., Bergantini, A., Turner, A. M., & Kaiser, R. I. 2018a, *ChPhC*, **19**, 556
- Abplanalp, M. J., Góbi, S., & Kaiser, R. I. 2019, *PCCP*, **21**, 5378
- Abplanalp, M. J., Gozem, S., Krylov, A. I., et al. 2016b, *PNAS*, **113**, 7727
- Abplanalp, M. J., Jones, B. M., & Kaiser, R. I. 2018b, *PCCP*, **20**, 5435
- Abplanalp, M. J., & Kaiser, R. I. 2017, *ApJ*, **836**, 195
- Abplanalp, M. J., & Kaiser, R. I. 2019, *PCCP*, **21**, 16949
- Abplanalp, M. J., & Kaiser, R. I. 2020, *ApJ*, **889**, 3
- Allamandola, L., Tielens, A., & Barker, J. 1989, *ApJS*, **71**, 733
- Arumainayagam, C. R., Garrod, R. T., Boyer, M. C., et al. 2019, *ChSRv*, **48**, 2293
- Bacmann, A., Taquet, V., Faure, A., Kahane, C., & Ceccarelli, C. 2012, *A&A*, **541**, L12
- Bernstein, M. P., Sandford, S. A., Allamandola, L. J., Chang, S., & Scharberg, M. A. 1995, *ApJ*, **454**, 327
- Boogert, A. C. A., Gerakines, P. A., & Whittet, D. C. B. 2015, *ARA&A*, **53**, 541
- Bottger, G. L., & Eggers, D. F., Jr. 1964, *JCP*, **40**, 2010
- Cané, E., Miani, A., Palmieri, P., Taroni, R., & Trombetti, A. 1997, *AcSpA*, **53**, 1839
- Cané, E., Miani, A., & Trombetti, A. 2007, *JPCA*, **111**, 8218
- Cernicharo, J., Marcelino, N., Roueff, E., et al. 2012, *ApJ*, **759**, L43
- Chuang, K. J., Fedoseev, G., Qasim, D., et al. 2017, *MNRAS*, **467**, 2552
- Cuppen, H. M., Walsh, C., Lamberts, T., et al. 2017, *SSRv*, **212**, 1
- Cuyille, S. H., Zhao, D., Strazzulla, G., & Linnartz, H. 2014, *A&A*, **570**, 1
- Doney, K. D., Zhao, D., Stanton, J. F., & Linnartz, H. 2018, *PCCP*, **20**, 5501
- Drouin, D., Couture, A. R., Joly, D., et al. 2007, *Scanning*, **29**, 92
- Duley, W. W., & Anming, H. 2009, *ApJ*, **698**, 808
- Dunning, T. H., Jr. 1989, *JCP*, **90**, 1007
- Eckhardt, A. K., Bergantini, A., Singh, S. K., Schreiner, P. R., & Kaiser, R. I. 2019, *Angew Chem Int Ed*, **58**, 5663
- Fedoseev, G., Cuppen, H. M., Ioppolo, S., Lamberts, T., & Linnartz, H. 2015, *MNRAS*, **448**, 1288
- Frisch, M. J., Trucks, G. W., Schlegel, H. B., et al. 2016, Gaussian 16, Revision C.01 (Wallingford CT: Gaussian Inc)
- Garrod, R. T., Wakelam, V., & Herbst, E. 2007, *A&A*, **467**, 1103
- Garrod, R. T., Weaver, S. L. W., & Herbst, E. 2008, *ApJ*, **682**, 283
- Gerakines, P. A., Moore, M. H., & Hudson, R. L. 2001, *JGRE*, **106**, 33381
- Gerakines, P. A., Schutte, W. A., Greenberg, J. M., & van Dishoeck, E. F. 1995, *A&A*, **296**, 810
- Gibb, E. L., Whittet, D. C. B., Boogert, A. C. A., & Tielens, A. G. G. M. 2004, *ApJS*, **151**, 35
- Gozem, S., Gunina, A. O., Ichino, T., et al. 2015, *JPCL*, **6**, 4532
- Gozem, S., & Krylov, A. I. 2018, ezDyson Version 4.1, <http://iopshell.usc.edu/downloads/ezdyson/>
- Gozem, S., Seidel, R., Hergenbahn, U., et al. 2020, *JPCL*, **11**, 5162
- Hagen, W., Allamandola, L. J., & Greenberg, J. M. 1979, *Ap&SS*, **65**, 215
- Harshbarger, W. R., Kuebler, N. A., & Robin, M. B. 1974, *JCP*, **60**, 345
- He, J., Emtiaz, S. M., & Vidalí, G. 2018, *ApJ*, **863**, 156
- Herbst, E. 2014, *PCCP*, **16**, 3344
- Herbst, E. 2017, *IRPC*, **36**, 287
- Hincelin, U., Wakelam, V., Hersant, F., et al. 2011, *A&A*, **530**, A61
- Hollis, J. M., Anthony, J. R., Jewell, P. R., & Lovas, F. J. 2006, *ApJ*, **642**, 933
- Hollis, J. M., Lovas, F. J., & Jewell, P. R. 2000, *ApJL*, **540**, L107
- Hudgins, D. M., & Sandford, S. A. 1998, *JPCA*, **102**, 329
- Hudson, R. L., Ferrante, R. F., & Moore, M. H. 2014, *Icar*, **228**, 276
- Hudson, R. L., & Gerakines, P. A. 2019, *MNRAS*, **482**, 4009
- Indriolo, N., & McCall, B. J. 2013, *ChSRv*, **42**, 7763
- Jaber Al-Edhari, A., Ceccarelli, C., Kahane, C., et al. 2017, *A&A*, **597**, A40
- Jamieson, C. S., Mebel, A. M., & Kaiser, R. I. 2006, *ApJS*, **163**, 184
- Jiménez-Serra, I., Vasyunin, A. I., Caselli, P., et al. 2016, *ApJ*, **830**, L6
- Kaiser, R. I. 2002, *ChRv*, **102**, 1309
- Kaiser, R. I., Eich, G., Gabrysich, A., & Roessler, K. 1997, *ApJ*, **484**, 487
- Kaiser, R. I., Maity, S., & Jones, B. M. 2014, *PCCP*, **16**, 3399
- Kaiser, R. I., & Roessler, K. 1997, *ApJ*, **475**, 144
- Kaiser, R. I., & Roessler, K. 1998, *ApJ*, **503**, 959
- Kim, Y. S., & Kaiser, R. I. 2009, *ApJS*, **181**, 543
- Kostko, O., Bandyopadhyay, B., & Ahmed, M. 2016, *ARPC*, **67**, 19
- Leroux, K., & Krim, L. 2021, *MNRAS*, **500**, 1188
- Loison, J.-C., Agúndez, M., Marcelino, N., et al. 2016, *MNRAS*, **456**, 4101
- Loomis, R. A., McGuire, B. A., Shingledecker, C., et al. 2015, *ApJ*, **799**, 34
- Maity, S., Kaiser, R. I., & Jones, B. M. 2014, *ApJ*, **789**, 36
- Majumdar, L., Gratier, P., Ruaud, M., et al. 2016, *MNRAS*, **466**, 4470
- Martin, J. M. L., & de Oliveira, G. 1999, *JCP*, **111**, 1843
- Martín-Doménech, R., Öberg, K. I., & Rajappan, M. 2020, *ApJ J.*, **894**, 98
- McGuire, B. A. 2018, *ApJS*, **239**, 17
- McGuire, B. A., Burkhardt, A. M., Kalenskii, S., et al. 2018, *Sci*, **359**, 202
- McMurtry, B. M., Saito, S. E. J., Turner, A. M., Chakravarty, H. K., & Kaiser, R. I. 2016, *ApJ*, **831**, 174
- Millar, T. J., Walsh, C., & Field, T. A. 2017, *ChRv*, **117**, 1765
- Moore, M. H., & Donn, B. 1982, *ApJ*, **257**, L47
- Moore, M. H., Ferrante, R. F., & Nuth, J. A. 1996, *P&SS*, **44**, 927
- Morton, R. J., & Kaiser, R. I. 2003, *P&SS*, **51**, 365
- Mozhayskiy, V. A., & Krylov, A. I. 2008, ezSpectrum, <http://iopshell.usc.edu/downloads/>
- Oana, C. M., & Krylov, A. I. 2007, *JCP*, **127**, 234106
- Oana, C. M., & Krylov, A. I. 2009, *JCP*, **131**, 124114
- Öberg, K. I., Bottinelli, S., Jørgensen, J. K., & van Dishoeck, E. F. 2010, *ApJ*, **716**, 825
- Öberg, K. I., Garrod, R. T., van Dishoeck, E. F., & Linnartz, H. 2009, *A&A*, **504**, 891
- Ortiz, J. V. 1999, *AdQC*, **35**, 33
- Paiva, M. A. M., Lefloch, B., & Galvão, B. R. L. 2018, *MNRAS*, **481**, 1858
- Purvis, G. D., III, & Bartlett, R. J. 1982, *JCP*, **76**, 1910
- Ruaud, M., Wakelam, V., & Hersant, F. 2016, *MNRAS*, **459**, 3756
- Sandford, S. A., Bernstein, M. P., & Allamandola, L. J. 2004, *ApJ*, **607**, 346
- Shao, Y., Gan, Z., Epifanovsky, E., et al. 2015, *MolPh*, **113**, 184
- Shingledecker, C. N., Álvarez-Barcia, S., Korn, V. H., & Kästner, J. 2019, *ApJ*, **878**, 80
- Shingledecker, C. N., & Herbst, E. 2018, *PCCP*, **20**, 5359
- Shingledecker, C. N., Le Gal, R., & Herbst, E. 2017, *PCCP*, **19**, 11043
- Shingledecker, C. N., Tennis, J., Gal, R. L., & Herbst, E. 2018, *ApJ*, **861**, 20
- Stanton, J. F., & Gauss, J. 1994, *JCP*, **101**, 8938
- Strazzulla, G., & Johnson, R. E. 1991, in *Comets in the Post-Halley Era*, ed. R. L. Newburn, Jr., M. Neugebauer, & J. Rahe (Dordrecht: Springer), 243
- Sullivan, K. K., Boamah, M. D., Shulenberg, K. E., et al. 2016, *MNRAS*, **460**, 664
- Terlouw, J. K., Holmes, J. L., & Lossing, F. P. 1983, *CajCh*, **61**, 1722
- Tielens, A. G. G. M. 2013, *RvMP*, **85**, 1021
- Tøomeng, E., Nielsen, C. J., Klaeboe, P., Hopf, H., & Priebe, H. 1980, *AcSpA*, **36**, 975
- van Dishoeck, E. F. 2014, *FaDi*, **168**, 9
- Vasyunin, A. I., & Herbst, E. 2013, *ApJ*, **769**, 34
- von Niessen, W., Bieri, G., & Åsbrink, L. 1980, *JESRP*, **21**, 175
- Wakelam, V., Loison, J. C., Herbst, E., et al. 2015, *ApJS*, **217**, 20
- Wu, Y.-J., & Cheng, B.-M. 2008, *ChPhL*, **461**, 53
- Yang, J., McCann, K., & Laane, J. 2004, *JMoSt*, **695**, 339
- Zhou, L., Kaiser, R. I., Gao, L. G., et al. 2008, *ApJ*, **686**, 1493
- Zhou, L., Kaiser, R. I., & Tokunaga, A. T. 2009, *P&SS*, **57**, 830
- Zhou, L., Zheng, W., Kaiser, R. I., et al. 2010, *ApJ*, **718**, 1243
- Zhu, C., Frigge, R., Bergantini, A., Fortenberry, R. C., & Kaiser, R. I. 2019, *ApJ*, **881**, 156